High precision laser ranging by time-of-flight measurement of femtosecond pulses

2012 Meas. Sci. Technol. 23 065203

(http://iopscience.iop.org/0957-0233/23/6/065203)

Meas. Sci. Technol. **23** (2012) 065203 (8pp) doi:10.1088/0957-0233/23/6/065203

High precision laser ranging by time-of-flight measurement of femtosecond pulses

Joohyung Lee, Keunwoo Lee, Sanghyun Lee, Seung-Woo Kim[1] and Young-Jin Kim[1]

Ultrafast Optics for Ultraprecision Group, Department of Mechanical Engineering, Korea Advanced Institute of Science and Technology (KAIST), Science Town, Daejeon, 305-701, Korea

E-mail: swk@kaist.ac.kr and yj.kim@kaist.ac.kr

Received 23 February 2012, in final form 3 April 2012
Published 4 May 2012
Online at stacks.iop.org/MST/23/065203

Abstract
Time-of-flight (TOF) measurement of femtosecond light pulses was investigated for laser ranging of long distances with sub-micrometer precision in the air. The bandwidth limitation of the photo-detection electronics used in timing femtosecond pulses was overcome by adopting a type-II nonlinear second-harmonic crystal that permits the production of a balanced optical cross-correlation signal between two overlapping light pulses. This method offered a sub-femtosecond timing resolution in determining the temporal offset between two pulses through lock-in control of the pulse repetition rate with reference to the atomic clock. The exceptional ranging capability was verified by measuring various distances of 1.5, 60 and 700 m. This method is found well suited for future space missions based on formation-flying satellites as well as large-scale industrial applications for land surveying, aircraft manufacturing and shipbuilding.

Keywords: time-of-flight, femtosecond laser, laser ranging

(Some figures may appear in colour only in the online journal)

1. Introduction

Distance is a fundamental physical quantity and the ability to measure distance with high precision is of primary importance in many fields of science and technology. Since Michelson's demonstration of optical interferometry for length measurement more than a century ago [1], the progress of optics has been central to advancing distance metrology with ever-growing demands on the measurement precision and range. The meter is the basic unit of distance and it is defined as the path traveled by light in a vacuum during a time interval of 1/299 792 458 of a second [2]. This time-interrelated definition of distance is based on the constancy and finiteness of the speed of light in a vacuum. This implies that the time-of-flight (TOF) of light pulses is the most direct measure of distance particularly in space. However, the achievable precision of TOF measurement has been limited by the bandwidth of the available photo-detection electronics, which is currently in the picosecond range or the equivalent of a few hundred micrometers in distance [3, 4]. Time gating with single-photon detectors or post-processing of TOF electric signals enables improvement in the measurement precision [5, 6]. Nonetheless, the fidelity of the converted electric pulse signal is degraded by the thermal phase drift as well as amplitude-to-phase conversion of photo-detection electronics, limiting the phase-detector resolution to a 0.1 ps level at best [7]. Consequently, TOF measurement was preferable only when measuring large distances with moderate precision as in geodetic surveying [8], range finders [9] and absolute altimeters [10]. For high precision ranging, optical interferometry has long been used as an alternative to TOF measurement because it relies on the wavelength of light as a ruler and subsequently provides sub-wavelength precision without the aid of high

[1] Authors to whom any correspondence should be addressed.

speed electronics. Nonetheless, optical interferometry is not suitable for measuring large distances because the periodic nature of light interference confines the non-ambiguity range to half the wavelength of light in principle. Employing multiple wavelengths by consecutive selection of different sources [11, 12] or by continuous sweeping of a tunable source [13] may extend the non-ambiguity range, but this synthetic approach increases the system complexity along with subsequent degradation in the attainable measuring speed and accuracy.

The recent progress of femtosecond pulse lasers pushes the limits of optical distance metrology in a number of respects [14]. The most notable progress is the precise wavelength calibration of continuous wave laser sources through the frequency comb of a femtosecond laser with direct reference to the atomic clock of well-defined absorption lines of atoms or molecules [15, 16]. Further, accurate optical frequencies can be generated actively by exploiting the frequency comb as a direct ruler, which subsequently leads to multi-wavelength interferometry with improved precision [17, 18] and also versatile coherent and incoherent schemes of absolute ranging [19, 20]. Other progress is the direct use of femtosecond lasers as light sources to measure large distances, which was first demonstrated by a synthetic wavelength interferometer that exploits a sequence of radio frequency (rf) harmonics of the pulse repetition rate of a femtosecond laser [21]. This attempt was followed by the proposition of a TOF measurement of femtosecond pulses by incorporating coherence interferometry to achieve high precision for the large distance ranging demanded for future space missions [22, 23]. Incoherent TOF measurement was also demonstrated with the aid of balanced optical cross-correlation [24]. Dispersive interferometry using a femtosecond laser was also introduced for absolute distance measurement by collective processing of an abundance of interference signals of the frequency comb [25, 26]. The dispersive approach was further refined by adopting the multi-heterodyne principle using a pair of frequency combs, which enabled improved measurement precision and speed [27]. All these attempts were aimed at extending the high precision of optical interferometry to longer distances using the frequency comb of femtosecond lasers.

In this paper, we continue to discuss about the non-interferometric method which we first proposed in [24] for high precision ranging based on TOF measurement of femtosecond pulses. The method overcomes the limited bandwidth of photo-detection electronics by means of balanced optical cross-correlation. Here the measurement principle is explained in further detail with experimental results for short, medium and long distances (1.5, 60 and 700 m) obtained in the air.

2. High precision TOF measurement

Figure 1 shows the basic concept of the proposed precision laser ranging by TOF measurement of femtosecond pulses. The traditional TOF method based on direct detection of light pulses is not suitable for femtosecond pulses since the bandwidth of photo-detection electronics is limited to the picosecond range (see figure 1(*a*)). The electric signal

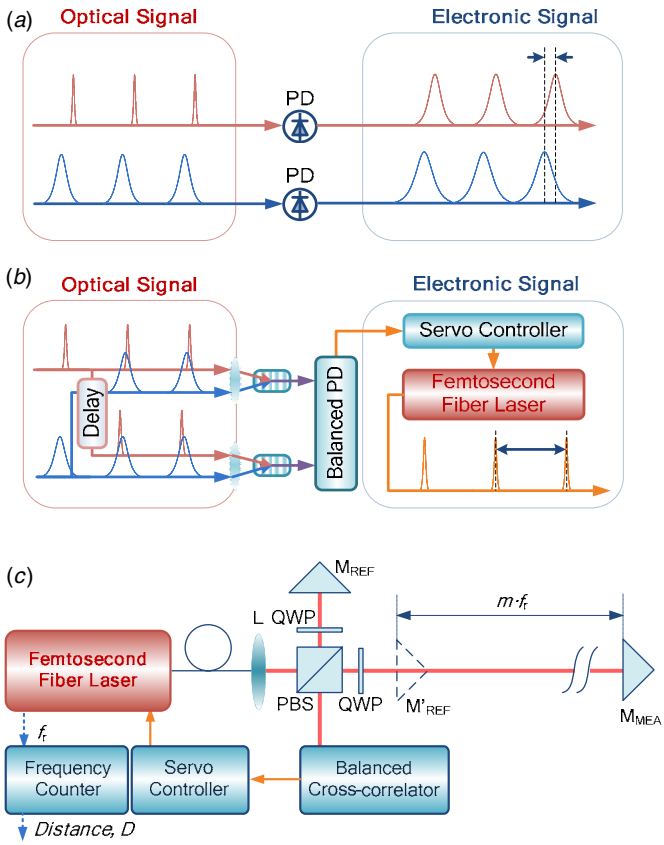

Figure 1. High precision TOF measurement of femtosecond light pulses. The measurement pulses returning from the retroreflector have a longer duration than that of the reference pulses due to dispersion in air. (*a*) Schematic of the conventional TOF measurement, (*b*) schematic of the balanced optical cross-correlation with femtosecond pulses, and (*c*) experimental configuration of the high precision laser ranging by balanced optical cross-correlation. PD: photo-detector, L: lens, M: mirror, QWP: quarter-wave plate, PBS: polarization beam splitter, DM: dichroic mirror.

obtained from photo-detection electronics suffers signal broadening. On the other hand, the optical cross-correlation technique converts the timing difference between two pulses into an optical signal without losing the femtosecond timing resolution [28–30]. For this purpose, as shown in figure 1(*b*), nonlinear optical crystals are exploited whose output intensity represents the instantaneous cross-correlation between two overlapping pulses. For balanced detection, another optical cross-correlation path is made in which the reference pulses are time-shifted by a pre-determined relative delay to the measurement pulses. Subtracting the two optical cross-correlation signals with a balanced photo-detector permits minimizing the unwanted drift and common noise. The balanced detection signal yields an s-shaped response to the temporal offset between the two pulse trains, whose central part offers the steepest slope of several mV fs^{-1} to be used as the error signal for feedback control; thereby the pulse repetition rate of the femtosecond laser source is precisely locked to maintain the error signal at zero constantly.

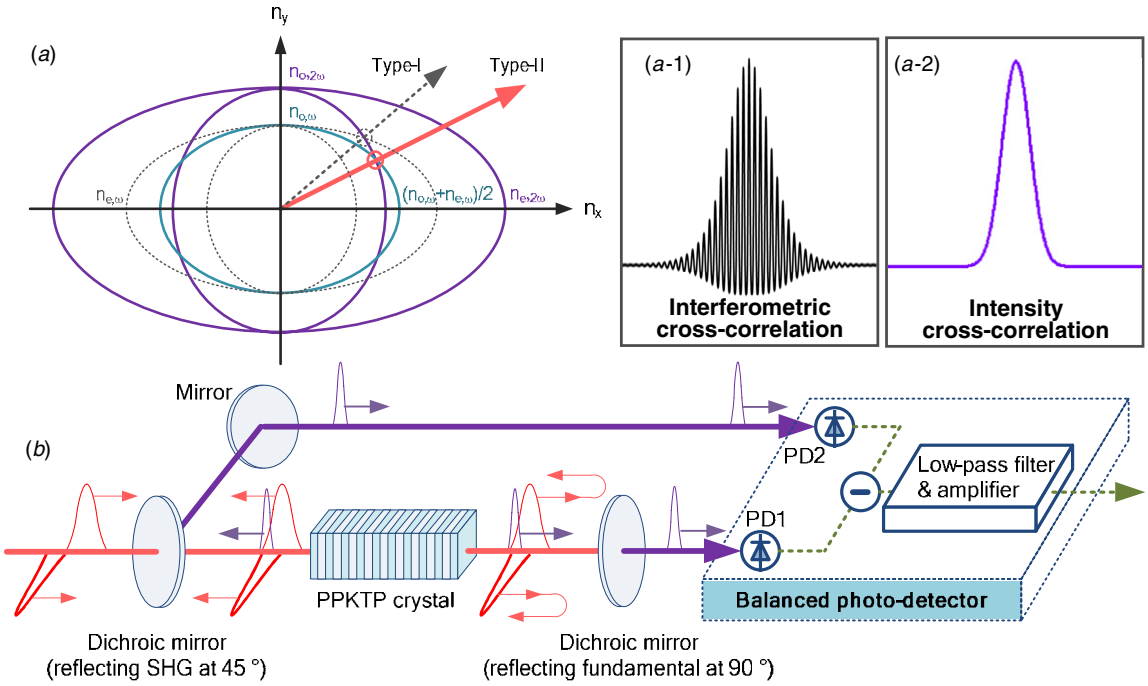

Figure 2. Balanced optical cross-correlation for TOF measurement. (*a*) Index ellipsoid of nonlinear crystals for optical cross-correlation, (*a*-1) fringe resolved interferometric cross-correlation, (*a*-2) intensity cross-correlation in the type-II PPKTP crystal, and (*b*) system layout for balanced optical cross-correlation.

When the reference and measurement pulses are locked with a zero temporal offset, the target distance can be expressed as

$$D = mc/(2f_rN). \quad (1)$$

In equation (1), D is the path difference between the reference and measurement arms, c is the speed of light in the vacuum, f_r is the pulse repetition rate and N is the group refractive index of air. In addition, m denotes an integer that indicates that the reference pulses overlap the measurement pulses with a lateral offset of m pulses. The integer m is readily determined by measuring the incremental shift t_d of the temporal offset between the reference and measurement pulses while the pulse repetition rate is moved between two known values of f_{r1} and f_{r2}:

$$m = t_d/(1/f_{r1} - 1/f_{r2}). \quad (2)$$

The repetition rates f_{r1} and f_{r2} are measured by use of a frequency counter and the incremental shift t_d is determined by monitoring the balanced s-shaped signal using a high resolution oscilloscope. In this procedure of determining m, no locking control of the repetition rate is needed.

Figure 1(*c*) illustrates the optical hardware system configured in this investigation. The femtosecond laser source is an Er-doped fiber laser (C-fiber, MenloSystems GmbH) that emits short pulses of a 1550 nm central wavelength with a 60 nm spectral bandwidth. The repetition rate is tunable in the range of $\pm$ 200 kHz about 100 MHz. The pulses are amplified to 240 mW using a home-built Er-doped fiber amplifier that consists of two 450 mW pump lasers at 980 nm and a 1.5 m long Er-doped fiber [31, 32]. The temporal pulse duration is 220 fs when measured after amplification. The pulses are split into two trains using a polarizing beam splitter (PBS): one is directed to the reference mirror M_{REF} and the other to the measurement mirror M_{MEA}. The measurement mirror is moved along the optical axis using a PZT actuator on a translational stage, whereas the reference mirror is fixed stationary.

As illustrated in figure 2(*b*), the reference and measurement pulses are recombined with orthogonal polarizations so that the temporal offset between the two pulse trains can be determined by means of optical cross-correlation. For this purpose, a 4 mm long periodically poled potassium titanyl phosphate (PPKTP) crystal is used, which has a poling period of 46.2 μm and a 100 nm phase matching bandwidth centered at a 1550 nm wavelength [29, 33]. The balanced photo-detector (PDB150A, Thorlabs) used here has a DC to 0.3 MHz bandwidth. Two dichroic mirrors are used; one reflects IR wavelengths near 1550 nm and transmits short second-harmonic (SH) wavelengths near 775 nm while the other does the opposite. On the reverse path, the reference pulses undergo a time-shift with respect to the measurement pulses by the birefringence effect of the PPKTP crystal. The error signal generated at the balanced cross-correlator by subtracting the two cross-correlation signals is transferred to a servo controller (LB1005, New Focus) that is connected to the PZT actuator installed inside the laser oscillator to vary the cavity length. This feedback control adjusts the repetition rate so as to lock the error signal to zero with a 6 kHz servo bandwidth. At the same time, the absolute distance of the target mirror is calculated from the pulse repetition rate following the relation of equation (1). The pulse repetition rate is measured

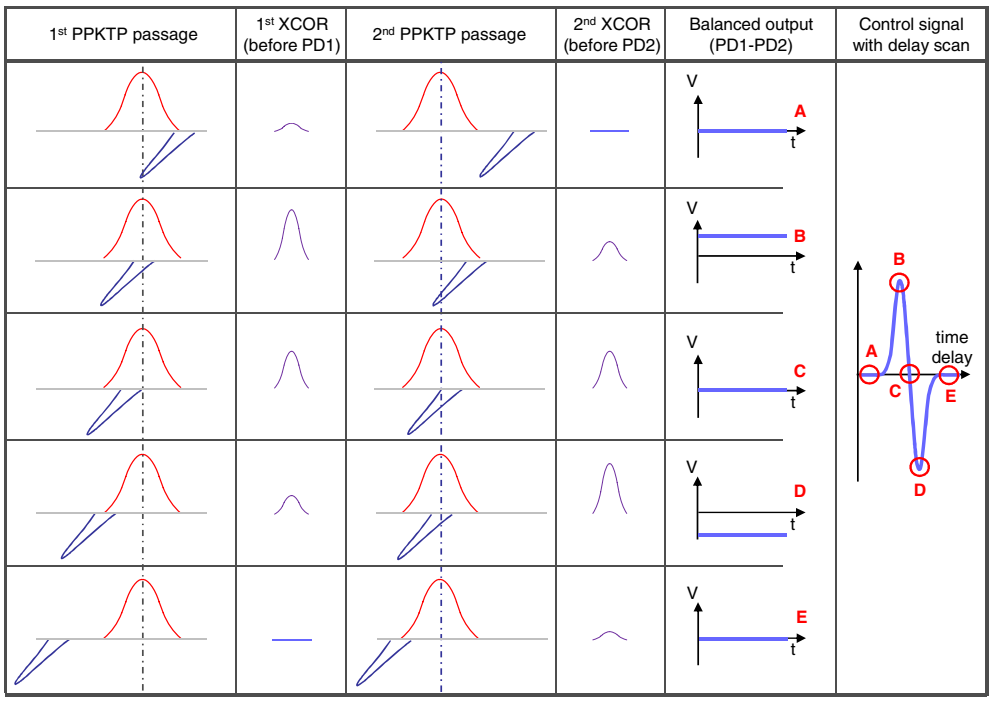

Figure 3. Generation of the balanced optical cross-correlation signal with varying temporal offset between the reference and measurement pulses.

by use of a high speed frequency counter (CNT-90, Pendulum Instruments) referenced to a Rb clock.

3. Balanced optical cross-correlation

The balanced cross-correlation (BCC) technique enables precise quantification of the temporal offset between the reference and measurement pulses. Type-II phase-matched PPKTP crystals produce a non-fringe resolved SH sub-pulse, denoted by $h_{CC}(\tau)$, whose intensity profile is proportional to the instantaneous overlap between the measurement pulse, $g_{mea}(t)$, and reference pulse, $f_{ref}(t)$. As depicted in figure 2(*a*-2), the SH sub-pulse can be expressed as [34]

$$h_{CC}(\tau) = (f_{ref} * g_{mea})(\tau) \equiv \int_{-\infty}^{\infty} f_{ref}^{*}(t) g_{mea}(t+\tau)\,dt. \quad (3)$$

It is worthwhile to note that the fringe resolved interferometric cross-correlation shown in figure 2(*a*-1) appears to offer a steeper zero-crossing slope than the non-fringe resolved signal of h_{CC}. However, the fringe resolved method requires continuous dithering of the reference mirror to detect the interferometric cross-correlation and suffers ambiguity in locating the true zero-crossing point due to many fringes arising during a pulse-overlap period. Consequently, the fringe resolved method is found to be unsuitable for the real-time absolute ranging pursued in our investigation.

For balanced optical detection of the signal h_{CC}, another SH sub-pulse is generated by reversing the main pulses using a dichroic mirror to propagate through the same crystal again with a relative time-shift induced by the birefringence of the PPKTP crystal (figure 2(*b*)). Then the two SH sub-pulses are converted into electrical signals using a pair of photo-detectors with subsequent electrical subtraction. The intensity of the BCC h_{CC} may be expressed as $I_0 \cdot h_{CC}$ with I_0 being the gain of electric photo-detection. Thus, its temporal variation can be written as

$$\Delta I_{CC}(\tau) = I_0 \frac{dh_{CC}(\tau)}{d\tau}\Delta\tau + h_{CC}(\tau)\Delta I_0. \quad (4)$$

The first term on the right-hand side of equation (4) represents the fluctuation caused by the distance variation given by $\Delta\tau$, and the second term denotes the amplitude noise affected by ΔI_0 [32]. The BCC technique of subtraction operation of $I_{BCC}(\tau) = I_0\{h_{CC}(\tau + \tau_0/2) - h_{CC}(\tau - \tau_0/2)\}$ gives the balanced output signal in the form of

$$\Delta I_{BCC}(\tau) = I_0\Delta\tau \cdot \left(\left.\frac{dh_{CC}(\tau)}{d\tau}\right|_{\tau+\tau_0/2} - \left.\frac{dh_{CC}(\tau)}{d\tau}\right|_{\tau-\tau_0/2} \right), + \Delta I_0 \cdot \{h_{CC}(\tau + \tau_0/2) - h_{CC}(\tau - \tau_0/2)\} \quad (5)$$

where τ_0 denotes the birefringence phase delay induced by the PPKTP crystal, which was measured to be 680 fs in our experiment. Equation (5) explains that the noise effect is canceled out by the subtraction operation. In consequence, the BCC technique offers a two-fold enhancement in obtaining the error signal with improvement not only in the sensitivity to $\Delta\tau$ but also in the immunity to noise and drift-free long-term stability. Figure 3 illustrates how the s-shaped BCC signal is generated with varying temporal offset between the reference and measurement pulses. The linear slope between points B and D in the s-curve is effectively used as the control signal to regulate the pulse repetition rate, which consequently permits the target distance to be converted to a frequency value in the rf-regime.

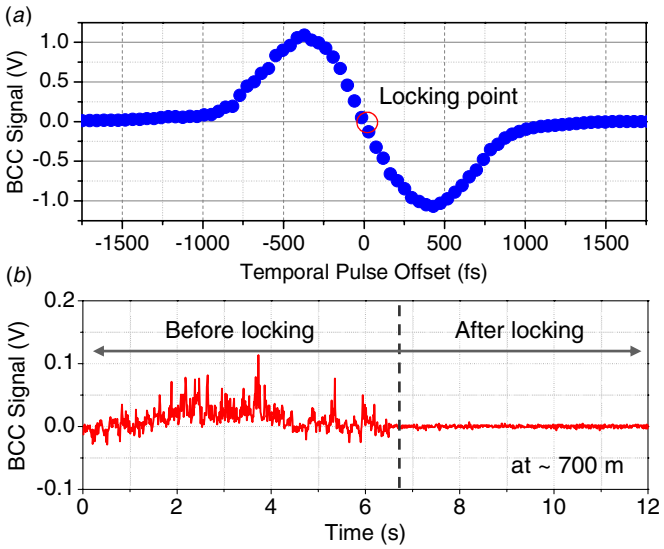

Figure 4. Balanced optical cross-correlation signal before and after locking control. (*a*) An exemplary s-shaped BCC signal, and (*b*) time-trace of the BCC signal before and after locking.

4. Locking performance

Figure 4(*a*) shows a typical pattern of the s-shaped BCC signal obtained in our experiment. The BCC signal provides a steep linear slope of 4.03 mV fs^{-1}, which is strong enough to control the repetition rate with a sub-fs level of timing jitter [29]. The temporal width of a single peak in the BCC signal was measured to be 530 fs in full width at half maximum, which was affected by the air dispersion in the round-trip path, input pulse duration and dispersion resulting from the optics in use. Detailed discussions on the broadening effect of the returning measurement pulses on the measurement accuracy are found in [24]. The repetition rate of the femtosecond laser was exemplarily locked to a target distance of ∼697.375 m using the BCC signal as shown in figure 4(*b*). Before the locking begins, the BCC signal yielded a fluctuation of 0.14 V over an interval of 6.2 s, which corresponds to a distance variation of 5.2 μm. After locking, the fluctuation of the BCC signal was stabilized to a level of ∼6.4 mV in standard deviation at a sampling rate of 1 ms. Large dispersion induced in the femtosecond pulses traveling a long air path needs to be actively compensated to avoid a significant degradation in the ranging precision [35]. However, for short distances less than several hundreds of meters, the pulse broadening effect was well pre-compensated simply by adding a single-mode fiber together with a dispersion-compensating fiber after the laser source.

5. Comparison with a conventional laser interferometer

The measurement performance of the developed apparatus was evaluated in comparison with a He–Ne laser interferometer (HP5501A, Hewlett Packard) at a target distance of ∼1.5 m ($m = 1$ in equation (1)). The target distance was measured while it was varied in steps of 0.5 μm. With an averaging time of 1 s, five measurements were taken in each step as shown in figure 5. The He–Ne laser interferometer was not capable of measuring the target distance in an absolute way; thus only incremental displacements between steps were compared as presented in figure 5. This test result clearly demonstrates that our method is capable of measuring the target distance in an absolute way with the same resolution as the He–Ne laser interferometer can provide only for measurement of relative displacements.

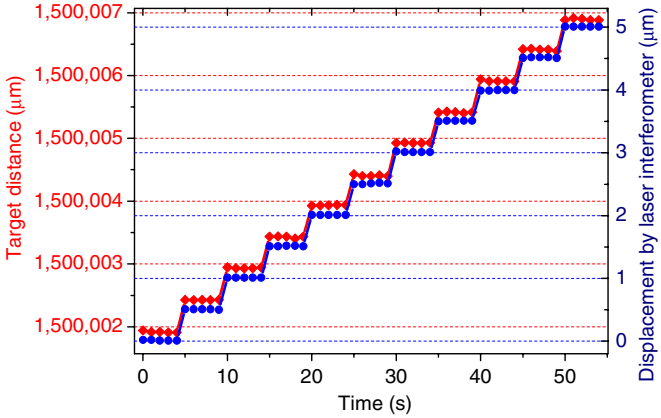

Figure 5. Comparison of the measurement result of the proposed apparatus with that of a conventional laser interferometer at a nominal distance of 1.5 m.

6. Absolute long distance measurement

The absolute ranging capability of the proposed system was further evaluated by measuring longer target distances of ∼60 m and ∼0.7 km. The beam diameter was expanded to 45 mm to facilitate the beam alignment to the target mirror for long distance measurements. For the given beam diameter, the eye-safe power limit is worked out to be 1.3 W in consideration of the maximum permissible exposure of 0.1 W cm^{-2} at 1550 nm wavelength. This calculation confirms that the amplified beam power of 240 mW used in our experiment is eye-safe with a large margin. Figure 6 shows the experimental setup and test results obtained with the target mirror located at a distance of ∼60 m from the measurement apparatus at the opposite end of a corridor. The target distance was then determined by reading the pulse repetition rate using a frequency counter. The data integration time was set to 5 ms as shown in figure 6(*b*). The pulse repetition rate was super-heterodyned to 400 kHz by mixing with a 100.4 MHz reference signal in order to attain more significant digits and a higher update rate. The group refractive index of air, N, was assumed constant during the experiment and compensated using the updated Edlen formula [36]. To quantify the measurement resolution, a 10 Hz sinusoidal distance modulation with a 1.0 μm amplitude was applied to the target mirror using a PZT actuator. Figure 6(*b*) shows that the given modulation was clearly resolved; the frequency and depth of modulation were measured to be 10 Hz and 0.9 μm, respectively, as plotted in figure 6(*c*).

The target distance was extended to ∼0.7 km by locating the target mirror on the top floor of a separate building. The

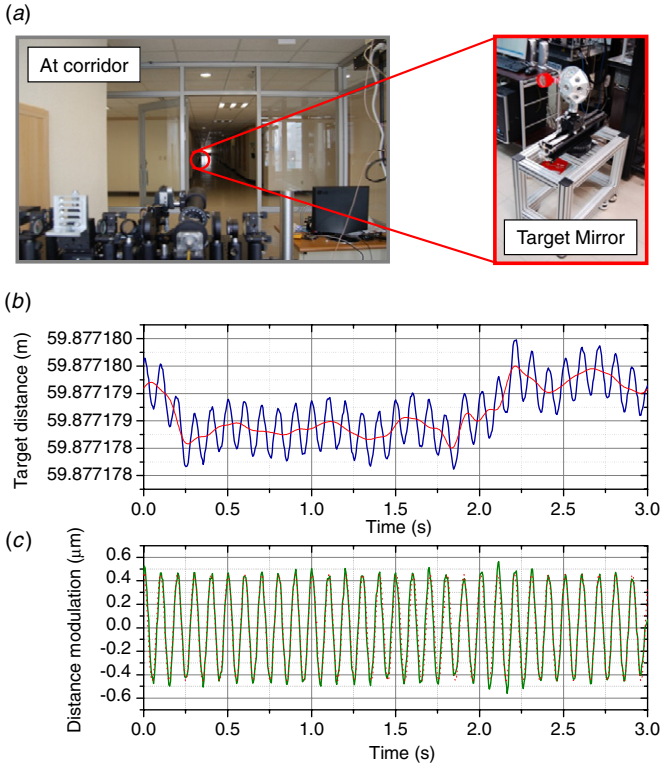

Figure 6. Demonstration of resolving capability for distance modulation at a target distance of ~60 m. (*a*) Photo of the experimental apparatus, (*b*) real-time tracing of the target distance, and (*c*) extracted sinusoidal modulation of the target distance.

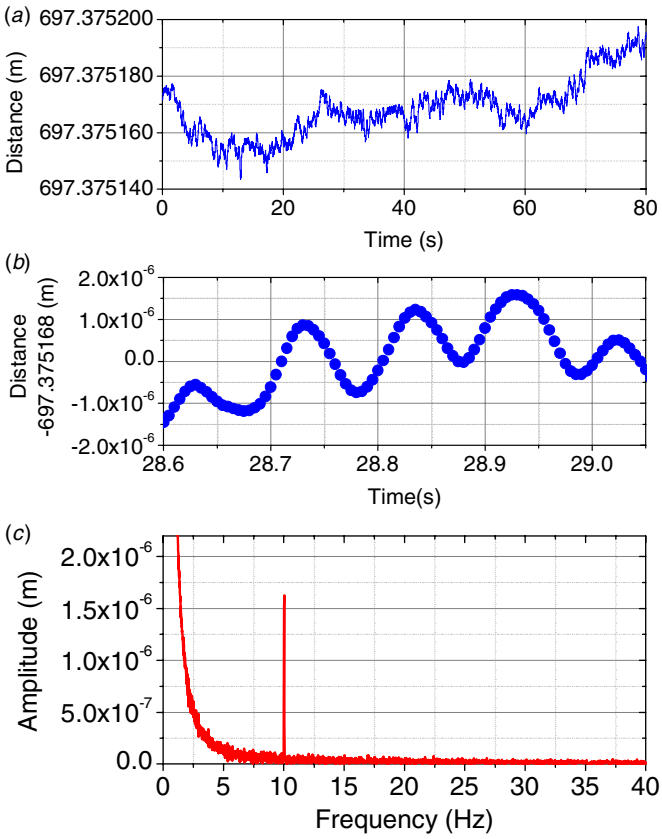

Figure 7. Long distance ranging: (*a*) measurement result of ~0.7 km, (*b*) magnified view to verify the measurement precision, and (*c*) Fourier transform spectrum analysis.

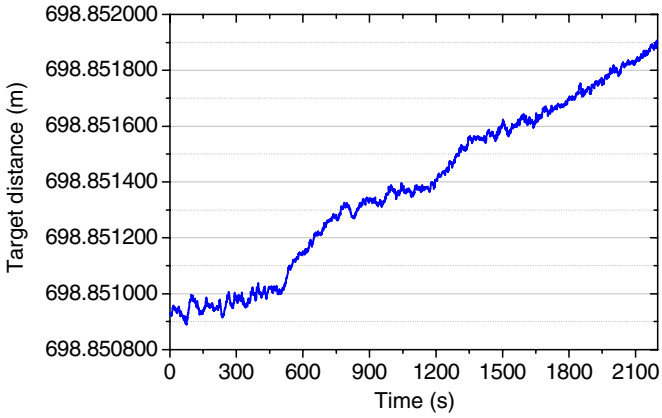

Figure 8. Long-term drift measurement of a target distance of ~0.7 km.

laser beam was emitted with an average power of 240 mW and returned with 15 mW from the target, which correspond to 1.87×10^{18} and 1.17×10^{17} photons per second, respectively. The temporal offset between the reference and measurement pulses was well maintained within 1.58 fs (at an integration time of 1 ms) throughout the experiment. The target mirror was also modulated at 10 Hz with a 1.6 μm amplitude, and the group refractive index of air was compensated as previously stated. The measured distance yielded an ~60 μm peak-to-valley variation during 80 s as shown in figure 7(*a*) at an integration time of 5 ms. The large fluctuation of the measured distance was presumed to be affected by the building vibration and also environmental change of the refractive index of air. Despite the ambient disturbance, the magnified view of the distance reading shown in figure 7(*b*) clearly demonstrates that the applied distance modulation was well resolved. Spectral analysis was then performed using the Fourier transform as shown in figure 7(*c*). Therein, the 10 Hz modulation with an ~1.6 μm amplitude was clearly seen along with a relatively broader low frequency variation below 5 Hz. The locked timing jitter at the corresponding integration time can be regarded as the ranging resolution, which scales down to 158 as corresponding to ~23.7 nm at an integration time of 100 ms.

The narrow tuning range of the pulse repetition rate results in dead-zones appearing in short distances where the reference and measurement pulses cannot overlap. The threshold distance for free dead-zones was estimated to be 187.5 m. This threshold distance could be shortened further by either increasing the tuning range or adopting higher repetition rate oscillators [37–39]. For example, a repetition rate of 800 MHz permits the threshold distance to reduce to 3 m, which is short enough for medium and long ranging applications.

The long-term drift of the measured target distance was continuously monitored without modulation for more than 30 min as shown in figure 8. The target optical path difference, $N \cdot D$, underwent a variation of 1.02 mm, which is comparable to the typical measuring resolution of conventional distance measuring devices based on TOF of light pulses. This confirms that our method of absolute ranging may be useful

for various scientific and industrial applications in terms of high precision, no ambiguity and high update rate. Besides, the measurement range is not affected by the coherence of the light source and the measured result is traceable to the time standard.

7. Conclusions

High precision ranging with femtosecond pulses was demonstrated without loss of femtosecond resolution with the aid of balanced optical cross-correlation. Target distances of 1.5, 60 and 700 m were measured with sub-micrometer precision with reference to a Rb atomic clock. Our method would be applicable for non-cooperative LIDAR or industrial targets with necessary power amplification. The outstanding performance of high precision ranging could allow future space missions to perform synthetic aperture imaging by deploying multiple satellites to orbit in tight formation [40–42] as well as traditional applications of TOF measurement in aerospace, shipbuilding and land surveying industries.

Acknowledgments

This work was supported by the National Space Laboratory Program, Global Research Network Program, Basic Science Research Program (2010-0024882) and Creative Research Initiative Program funded by the National Research Foundation of the Republic of Korea.

References

[1] Michelson A A and Morley E W 1887 On the relative motion of the earth and the luminiferous ether *Am. J. Sci.* **34** 333–45
[2] Giacomo P 1984 News from the BIPM *Metrologia* **20** 25–30
[3] Dickey J O *et al* 1994 Lunar laser ranging: a continuing legacy of the Apollo Program *Science* **265** 482–90
[4] Pellegrin S, Buller G S, Smith J M, Wallace A M and Cova S 2000 Laser-based distance measurement using picosecond resolution time-correlated single-photon counting *Meas. Sci. Technol.* **11** 712–6
[5] Wallace A M, Ye J, Krichel N J, McCarthy A, Collins R J and Buller G S 2010 Full waveform analysis for long-range 3D imaging laser radar *EURASIP J. Adv. Signal Process.* **2010** 806708
[6] Albota M A *et al* 2002 Three-dimensional imaging laser radars with Geiger-mode avalanche photodiode array *Linc. Lab. J.* **13** 351–70
[7] Ivanov E N, Diddams S A and Hollberg L 2005 Study of the excess noise associated with demodulation of ultra-short infrared pulses *Freq. Control* **52** 1064–74
[8] Pritchard M E and Simons M 2002 A satellite geodetic survey of large-scale deformation of volcanic centres in the central Andes *Nature* **418** 167–71
[9] Yeomans D K *et al* 2000 Radio science results during the NEAR–Shoemaker spacecraft rendezvous with Eros *Science* **289** 2085–8
[10] Smith D E, Zuber M T and Neumann G A 2001 Seasonal variations of snow depth on Mars *Science* **294** 2141–6
[11] Tilford C R 1977 Analytical procedure for determining lengths from fractional fringes *Appl. Opt.* **16** 1857–60
[12] Dändliker R, Thalmann R and Prongué D 1988 Two-wavelength laser interferometry using superheterodyne detection *Opt. Lett.* **13** 339–41
[13] Kikuta H, Iwata K and Nagata R 1986 Distance measurement by the wavelength shift of laser diode light *Appl. Opt.* **25** 2976–80
[14] Kim S W 2009 Combs rule *Nature Photon.* **3** 313–4
[15] Jones D J, Diddams S A, Ranka J K, Stentz A, Windeler R S, Hall J L and Cundiff S T 2000 Carrier-envelope phase control of femtosecond mode-locked lasers and direct optical frequency synthesis *Science* **288** 635–9
[16] Holzwarth R, Udem T, Hansch T W, Knight J C, Wadsworth W J and Russell P S J 2000 Optical frequency synthesizer for precision spectroscopy *Phys. Rev. Lett.* **85** 2264–7
[17] Jin J, Kim Y J, Kim Y and Kim S W 2006 Absolute length calibration of gauge blocks using optical comb of a femtosecond pulse laser *Opt. Express* **14** 5968–74
[18] Schuhler N, Salvade Y, Leveque S, Dandliker R and Holzwarth R 2006 Frequency comb-referenced two-wavelength source for absolute distance measurement *Opt. Lett.* **31** 3101–3
[19] Schibli T R, Minoshima K, Bitou Y, Hong F L, Inaba H, Onae A and Matsumoto H 2006 Displacement metrology with sub-pm resolution in air based on a fs-comb wavelength synthesizer *Opt. Express* **14** 5984–93
[20] Hyun S, Kim Y J, Kim Y, Jin J and Kim S W 2009 Absolute length measurement with the frequency comb of a femtosecond laser *Meas. Sci. Technol.* **20** 095302
[21] Minoshima K and Matsumoto H 2000 High-accuracy measurement of 240 m distance in an optical tunnel by use of a compact femtosecond laser *Appl. Opt.* **39** 5512–7
[22] Ye J 2004 Absolute measurement of long, arbitrary distance to less than an optical fringe *Opt. Lett.* **29** 1153–5
[23] Cui M, Schouten R N, Bhattacharya N and van den Berg S A 2008 Experimental demonstration of distance measurement with a femtosecond frequency comb laser *J. Eur. Opt. Soc.* **3** 08003
[24] Lee J, Kim Y J, Lee K, Lee S and Kim S W 2010 Time-of-flight measurement with femtosecond light pulses *Nature Photon.* **4** 716–20
[25] Joo K N and Kim S W 2006 Absolute distance measurement by dispersive interferometry using a femtosecond pulse laser *Opt. Express* **14** 5954–60
[26] Joo K N, Kim Y and Kim S W 2008 Distance measurements by combined method based on a femtosecond pulse laser *Opt. Express* **16** 19799–806
[27] Coddington I, Swann W C, Nenadovic L and Newbury N R 2009 Rapid and precise absolute distance measurements at long range *Nature Photon.* **3** 351–6
[28] Schibli T R, Kim J, Kuzucu O, Gopinath J T, Tandon S N, Petrich G S, Kolodziejski L A, Fujimoto J G, Ippen E P and Kartner F X 2003 Attosecond active synchronization of passively mode-locked lasers by balanced cross correlation *Opt. Lett.* **28** 947–9
[29] Kim J, Chen J, Zhang J, Wong F N C, Kartner F X, Loehl F and Schlarb H 2007 Long-term femtosecond timing link stabilization using a single-crystal balanced cross correlator *Opt. Lett.* **32** 1044–6
[30] Kim J, Cox J A, Chen J and Kartner F X 2008 Drift-free femtosecond timing synchronization of remote optical and microwave sources *Nature Photon.* **2** 733–6
[31] Kim Y, Kim S, Kim Y J, Hussein H and Kim S W 2009 Er-doped fiber frequency comb with mHz relative linewidth *Opt. Express* **17** 11972–7
[32] Kim Y, Kim Y J, Kim S and Kim S W 2009 Er-doped fiber comb with enhanced f_{ceo} S/N ratio using Tm:Ho-doped fiber *Opt. Express* **17** 18606–11

[33] Konig F and Wong N C 2004 Extended phase matching of second-harmonic generation in periodically poled $KTiOPO_4$ with zero group-velocity mismatch *Appl. Phys. Lett.* **84** 1644–6
[34] Yoshitomi D, Kobayashi Y, Kakehata M, Takeda H and Torizuka K 2006 Synchronization of Ti:sapphire and Cr:forsterite mode-locked lasers with 100-attosecond precision by optical phase stabilization *Opt. Express* **14** 6359–65
[35] Lee S H, Lee J, Kim Y J, Lee K and Kim S W 2011 Active compensation of large dispersion femtosecond pulses for precision laser ranging *Opt. Express* **19** 4002–8
[36] Birch K P and Downs M J 1993 An updated Edlén equation for the refractive index of air *Metrologia* **30** 155–62
[37] Washburn B R, Fox R W and Newbury N R 2004 Low-noise fiber-laser frequency combs *Opt. Express* **12** 4999–5004
[38] Chen J, Sickler J W, Fendel P, Ippen E P, Kartner F X, Wilken T, Holzwarth R and Hansch T W 2008 Generation of low-timing-jitter femtosecond pulse trains with 2 GHz repetition rate via external repetition rate multiplication *Opt. Lett.* **30** 959–61
[39] Fortier C, Kibler B, Fatome J, Finot C, Pitois S and Millot G 2008 All-fibered high-quality low duty-cycle 160 Ghz femtosecond pulse source *Laser Phys. Lett.* **5** 817–20
[40] White N 2000 X-ray astronomy—imaging black holes *Nature* **407** 146–7
[41] Lawson P R and Dooley J A 2005 Technology plan for the terrestrial planet finder interferometer *Jet Propulsion Laboratory Publication 05-5* pp 1–149
[42] Fridlund C V M 2008 Future space missions to search for terrestrial planets *Space Sci. Rev.* **135** 355–69